RSC Advances

PAPER

View Article Online
View Journal | View Issue

Cite this: *RSC Adv.*, 2015, **5**, 19970

Insight into C + O(OH) reaction for carbon elimination on different types of CoNi(111) surfaces: a DFT study†

Xiaoqiang Guo,[a] Hongyan Liu,[b] Baojun Wang,*[a] Qiang Wang[c] and Riguang Zhang*[a]

A density-functional theory (DFT) method has been performed to investigate the reaction of C + O(OH) on three types of bimetallic alloy CoNi(111) surface, and the results obtained are compared with those on the pure Ni(111) surface. Our results show that the introduction of Co into the Ni catalyst is beneficial for the adsorption of C, O and OH species, while it weakens the adsorption of CO. Moreover, O(OH) absorbs preferentially on the CoNi(111) surfaces with the surface enrichment of Co compared with the homogeneous CoNi(111) surface; the increased degree of O adsorption energy outweighs the corresponding values of C on the pure Ni(111) and three types of bimetallic alloy CoNi(111) surfaces, indicating that Co has a stronger affinity for oxygen species than for carbon species. On the other hand, the mechanism of the C + O(OH) reaction and the corresponding rate constants at different temperatures show that OH species have a stronger ability to eliminate carbon than O species on Ni(111) and CoNi(111) surfaces; on the CoNi(111) surface, when the Co surface coverage is equal to 1 monolayer (ML), compared to Ni(111), the C + O reaction can be accelerated. When the Co surface coverage is equal to 3/4 ML, the C + OH reaction is the most favorable; further, the rate constant for the C + OH reaction on a CoNi(111) with Co surface coverage of 3/4 ML is much larger than that of the C + O reaction on a CoNi(111) with Co surface coverage of 1 ML. As a result, for carbon elimination on the CoNi alloy surface, OH species should serve as the key species for carbon elimination, and the Co surface coverage of CoNi(111) surface should be kept at 3/4 ML.

Received 1st December 2014
Accepted 4th February 2015

DOI: 10.1039/c4ra15555f

www.rsc.org/advances

1. Introduction

Catalytic reforming of CH_4 with CO_2 is exceptionally attractive from the environmental and economical points of view,[1–7] since this process can provide a potential way to utilize two abundant greenhouse gases as the building blocks for producing synthesis gas with a ratio of unity, which is very beneficial for the synthesis processes of some liquid fuels. A supported-Ni catalyst is regarded as the most attractive catalyst for this process. However, the rapid accumulation of coke on the catalyst and coke-induced deactivation are the main drawbacks preventing its application.[8,9]

Coke accumulation on the catalyst is the result of carbon formation and carbon removal. Thus, the avoidance of coking requires maximal rates of carbon removal and the minimization of one or more of the processes leading to carbon formation.[10] An effective way to suppress coke accumulation is to increase the feed CO_2/CH_4 ratio, and add the appropriate amount of steam, which can result in higher rates of carbon removal and can improve the stability.[11,12] It is widely accepted that the role of CO_2 or H_2O is to provide an oxidizer of CHx ($x = 1$–3) species, *i.e.*, O and OH species.[13,14] Previous studies have proposed that the oxygen intermediates, such as O and OH species, act largely as surface cleaners to scavenge the deposited carbon, further restoring the catalyst activity.[15–17] Thus, both C + O and C + OH reactions are believed to be the key steps in understanding carbon elimination.

A large number of studies have shown that surface O species originating from CO_2 dissociation are the key intermediates for carbon elimination, however, only a little attention has been paid to the OH species; for example, the studies by Ferreira-Aparicio *et al.*[18] have shown that surface OH species may play a key role in its resistance to deactivation by significantly decreasing the rate of carbon deposition on the metal. Meanwhile, based on isotopic TPO experiments, Goula *et al.*[19] assumed that OH species derived from the dissociation of adsorbed H_2O can participate in the carbon removal. By means of density functional theory (DFT) calculations, Shishkin and

[a]*Key Laboratory of Coal Science and Technology of Ministry of Education and Shanxi Province, Taiyuan University of Technology, No. 79 Yingze West Street, Taiyuan 030024, Shanxi, P.R. China. E-mail: quantumtyut@126.com; wangbaojun@tyut.edu.cn; zhangriguang@tyut.edu.cn; Fax: +86 351 6041237; Tel: +86 351 6018239*

[b]*College of Chemistry and Environment Engineering, Shanxi Datong University, Datong, Shanxi 037009, P.R. China*

[c]*State Key Laboratory of Coal Conversion, Institute of Coal Chemistry, Chinese Academy of Sciences, Taiyuan 030001, Shanxi, P.R. China*

† Electronic supplementary information (ESI) available. See DOI: 10.1039/c4ra15555f

Ziegler[20] have shown that OH species from adsorbed H_2O interact favorably with C to form CO species. According to their microkinetic analysis of dry reforming, Maestri *et al.*[13] have reported that CH_4 consumption proceeds *via* pyrolysis and carbon oxidation by the superficial OH species, which is consistent with the previous DFT slab calculations that C oxidation by OH species is more favorable than that by O species.[14,21] The above studies show that OH species may serve as the key species for carbon elimination. Therefore, insight into the promotional effect of OH species on carbon removal is evidently needed.

Nowadays, there is much research directed towards improving the stability and coking resistance of Ni-based catalysts. It has been suggested that bimetallic catalysts can improve the performance of activity and stability compared to the corresponding monometallic catalysts.[22,23] In particular, Co–Ni bimetallic catalysts have been proved to display a distinctive carbon-resistance ability and excellent catalytic performance. Co has also received much attention as an active metal for the catalytic reforming of CH_4 with CO_2. Compared to Ni-based catalysts, supported Co catalysts can exhibit a high tolerance to carbon deposition but gradually deactivate because of oxidation,[24,25] implying that they have a stronger affinity for oxygen species derived from CO_2 than carbon species. The combination of the oxygenophile nature of Co with that of Ni (stronger affinity for carbon species) is beneficial for reducing the possibility of metal oxidation and suppressing carbon formation. It is speculated that, by accelerating CH_4 decomposition, Ni provides the reductive hydrogen to Co *via* spillover phenomena,[26,27] which can inhibit the oxidation of the Co. Koh *et al.*[28] have found that the presence of Ni increases the reducibility of Co_3O_4 to Co, and the existence of Co leads to a decrease in the rate of coke formation by catalyzing the oxidation of surface carbon. Zhang and co-workers[29] have reported that a Co–Ni bimetallic catalyst with an approximate Co/Ni ratio of one can completely eliminate carbon for up to 250 h. However, the beneficial effects of bimetallic catalysts on carbon elimination remain unsolved, and need to be clarified.

On the other hand, the arrangement of the active component and the morphology of the CoNi surface are obviously affected by the reacting atmosphere, and the coexistence of reductive (CH_4, H_2, CO) and oxidative (CO_2, H_2O) species. Meanwhile, Co tends to form homogeneous structures with Ni,[30,31] or segregate on Ni surfaces,[29,32,33] and as a result, the modification of the surface morphology will in turn have an effect on the adsorption properties of key intermediates, and further on the reactivity of the deposited carbon with oxygen intermediates.[25,30] However, up to now, studies of the C + O(OH) reaction for carbon elimination on CoNi alloys are still scarce. In our previous work,[34] we have investigated the C + O reaction on a homogeneous CoNi(111) surface, but the promotional effect of OH species on carbon elimination has not been considered. More importantly, for the segregated CoNi surface, the underlying mechanisms of the reaction of carbon elimination and the effect of CoNi surface properties on carbon elimination have not been investigated.

In this study, a systematic DFT study of carbon elimination on three kinds of CoNi(111) surface, including a homogeneous surface, a surface with moderate segregation of Co, and a surface with excessive segregation of Co, has been performed to determine the reaction mechanism of carbon elimination. The adsorption geometries and energetics involved in carbon elimination on the three types of CoNi(111) surface are firstly discussed, and then the reactions of C + O and C + OH are investigated to elucidate the effects of Co and the structural properties of the CoNi surface on the carbon elimination performance.

2. Computational details

2.1 Surface models

Previous studies have shown that th supported CoNi bimetallic catalysts with an approximate Ni/Co ratio of one can provide the best catalytic activity, along with the absence of coking in the reforming of CH_4 with CO_2.[29,35] According to XRD analysis, the formation of a homogeneous alloy from the bulk to the surface has been observed.[31] Further, EXAFS fitting results suggested the formation of an ordered and homogeneous fcc Co–Ni alloy with Ni $\geq$ 50%.[36] Therefore, the CoNi binary system with a Ni/Co ratio of one is simulated by replacing two Ni atoms in the conventional cell of the four Ni atoms with two Co atoms. The equilibrium lattice constants of the NiCo alloy are optimized to be $a = 3.480$ Å, $b = c = 3.604$ Å.

The surfaces are obtained by cutting the NiCo alloy along the [111] direction. A rectangular (2×2) supercell with eight metal atoms in each layer is used to represent the CoNi(111) surface. Meanwhile, a 12 Å vacuum slab is employed to separate the periodically repeated slabs. The first Brillouin zone of the CoNi(111) surface is sampled with a $4 \times 4 \times 1$ *k*-point mesh. The bottom two layers in the slab models are constrained, and the upper two layers together with the adsorbed species are allowed to relax during all calculations. Herein, we set up the homogeneous CoNi(111) surface, which is denoted as Model A, as shown in Fig. 1. However, since the reacting atmosphere has an obvious effect on the structures of the CoNi surface, Co is prone to segregation on the surface, and as a result, another two models are constructed to represent the segregation of Co on the CoNi(111) surface: one is that resulting from exchanging two interval Ni atoms on the surface layer with two Co atoms on the subsurface layer; the other is that resulting from exchanging four surface Ni atoms with the four Co atoms on the subsurface layer, which are called as Model B and Model C, respectively (shown in Fig. 1). From Models A–C, the numbers of Co atoms presented on the surface layer are 4, 6 and 8, which corresponds to Co surface coverages of 1/2, 3/4 and 1 ML, respectively, *i.e.*, Model A represents the homogeneous surface, Model B presents the surface with moderate segregation of Co, and Model C presents the surface with excessive segregation of Co.

2.2 Computational methods

All DFT calculations in this study have been carried out using the Vienna *ab initio* simulation package (VASP).[37–39] The ionic

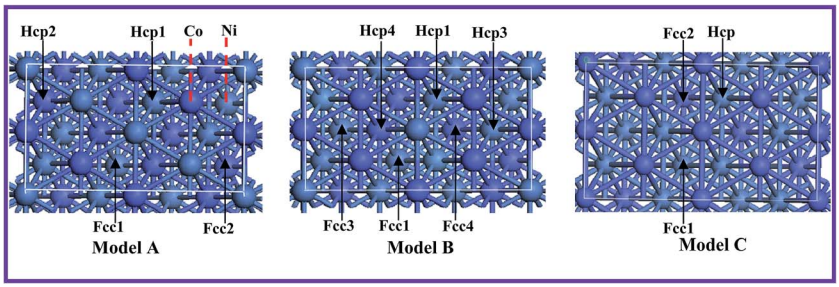

Fig. 1 The adsorption sites on Models A–C of CoNi(111) surface. Light sky blue balls represent Ni atoms, and neon blue balls represent Co atoms.

cores and their interaction with the valence electrons are described by the projector augmented wave method (PAW)[40,41] with a frozen-core approximation. The Kohn–Sham one-electron valence states are expanded in a basis of plane waves with a kinetic energy cutoff of 400 eV. The exchange–correlation energy is described with the Perdew–Burke–Ernzerhof (PBE)[42] scheme by using the generalized gradient approximation (GGA). Brillouin zone sampling is performed using a Monkhorst–Pack grid,[43] and electronic occupancies are determined according to Methfessel–Paxton scheme[44] with an energy smearing of 0.1 eV. Since the two magnetic elements Ni and Co are involved in the system, the spin-polarized effect has been considered. The relaxation of the electronic degrees of freedom is assumed to be converged if the total energy change and the band structure energy change between two steps are both smaller than 10^{-6} eV Å^{-1}. A force difference between two steps less than 0.01 eV Å^{-1} is used as the criterion for convergence of relaxation. Our calculated lattice constant of Ni (3.518 Å) agrees with the previous theoretical values (3.522 Å)[45] and the experimental value (3.52 Å).[46]

Reaction paths have been investigated using the climbing-image nudged elastic band method (CI-NEB).[47,48] Transition states have been optimized using the dimer method.[49,50] The transition state structure is thought to be converged when the forces acting on the atoms are all less than 0.05 eV Å^{-1} for the various degrees of freedom set in the calculation.

The adsorption energy, E_{ads}, is defined as follows:

$$E_{ads} = E_{(adsorbate/slab)} - E_{slab} - E_{adsorbate}$$

where $E_{(adsorbate/slab)}$ is the total energies of adsorbate on the slab model, E_{slab} is the total energy of the clean slab model. $E_{adsorbate}$ is the total energy of the isolated adsorbate obtained in a 10 × 10 × 10 Å cubic cell.

3. Results and discussion

3.1 Adsorption of reaction intermediates

In order to obtain the most stable adsorption configurations of related species involved in carbon elimination, various adsorption sites on the pure Ni(111) and the alloyed CoNi surfaces have been considered. There are four sites on the pure Ni(111) surface: top (T), bridge (B), hexagonal-close-packed (Hcp) and face-centered-cubic (Fcc). On the alloyed CoNi(111) surface, several new adsorption sites are formed due to the existence of two constituents in the lattice. According to the previous calculations on Ni(111),[14,21,51] the intermediates related to carbon elimination preferentially absorb at the Fcc and Hcp sites. Therefore, the threefold hollow sites of the alloyed CoNi surface are considered and highlighted in Fig. 1. Fig. 2 presents the stable adsorption configurations of the related species involved in carbon elimination on the Ni(111) surface. Our calculated adsorption sites for different adsorbates on Ni(111) are in good agreement with the previously reported values.[14,21] The calculated adsorption energies for all possible species at

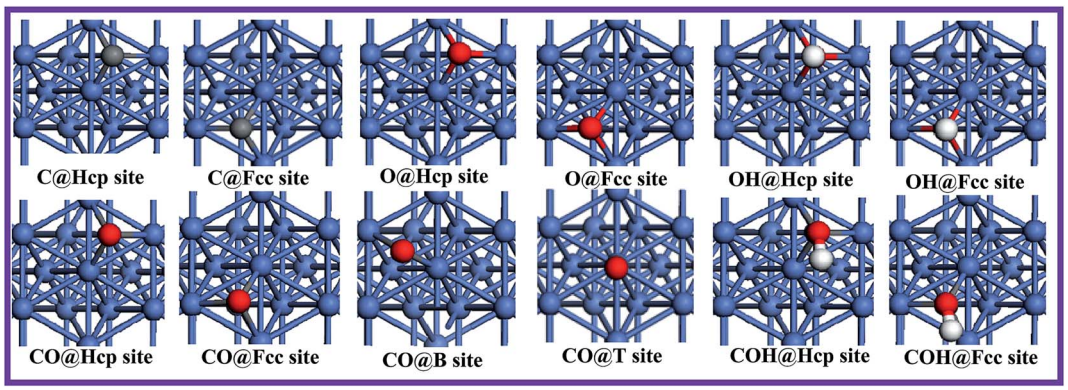

Fig. 2 The stable adsorption configurations of the species related to carbon elimination on the Ni(111) surface. Grey, white and red balls represent C, H and O atoms, respectively.

Table 1 Calculated adsorption energies (eV) of the species related to carbon elimination on the three types of alloyed CoNi(111) and the pure Ni(111) surfaces. The energies in bold are the corresponding adsorption energies at the most stable adsorption sites

	Ni(111)		CoNi(111)												
			Model A				Model B						Model C		
Species	Hcp	Fcc	Hcp1	Hcp2	Fcc1	Fcc2	Hcp1	Hcp3	Hcp4	Fcc1	Fcc3	Fcc4	Hcp	Fcc1	Fcc2
C	**−6.88**	−6.83	**−6.98**	−6.84	−6.83	−6.66	−7.04	**−7.06**	−6.88	−6.88	−6.91	−6.89	**−7.12**	−6.98	−6.97
O	−5.64	**−5.76**	**−5.99**	−5.73	−5.97	−5.74	−5.97	**−6.12**	−5.91	−5.98	−6.09	−5.98	**−6.86**	−6.72	−6.70
OH	−3.35	**−3.45**	−3.64	−3.42	**−3.68**	−3.44	−3.63	−3.79	−3.55	−3.65	−3.79	−3.69	−3.75	**−3.78**	−3.76
COH	**−4.39**	**−4.39**	**−4.35**	−4.32	−4.10	−4.22	**−4.43**	−4.39	−4.40	−4.40	−4.39	−4.40	**−4.49**	−4.45	−4.43
CO	**−1.89**	−1.87	−1.74	**−1.77**	−1.73	−1.69	**−1.79**	−1.76	−1.76	−1.78	−1.74	−1.76	**−1.82**	−1.78	−1.74
	−1.76[b]	−1.53[a]	−1.70[d]	−1.46[a]	−1.72[c]		−1.48[a]	−1.68[c]					−1.72[c]		

[a] The adsorption energies for CO at the top-Ni. [b] The adsorption energies for CO at the Ni–Ni bridge. [c] The adsorption energies for CO at the top-Co. [d] The adsorption energies for CO at the Ni–Co bridge.

the threefold hollow sites on the three types of CoNi(111) surface models are summarized in Table 1, and the corresponding adsorption structures are shown in Fig. 3–5, respectively.

3.1.1 C adsorption. Our results show that the initial configurations of C atoms adsorbed at the bridge and top sites on the Ni(111) surface are optimized into that at the threefold site after geometry optimization. On the CoNi(111) surface, the most favorable site on Model A is the Hcp1 site, while it is the Hcp3 site on Model B, and the Hcp site on Model C. The adsorption energy of Model C is −7.12 eV, it is slightly more negative by 0.06 eV than that of Model B, and by 0.14 and 0.24 eV than those of Model A and the Ni(111) surface, respectively, indicating that the introduction of Co leads to the increase of C adsorption stability compared to the pure Ni(111) surface.

3.1.2 O adsorption. Similar to C adsorption on Ni(111), O atoms located at the top site and bridge sites are inclined to transfer to the threefold site after geometry optimization. The most stable site for O species on Ni(111) is found to be the Fcc site with an adsorption energy of −5.76 eV, which is more stable

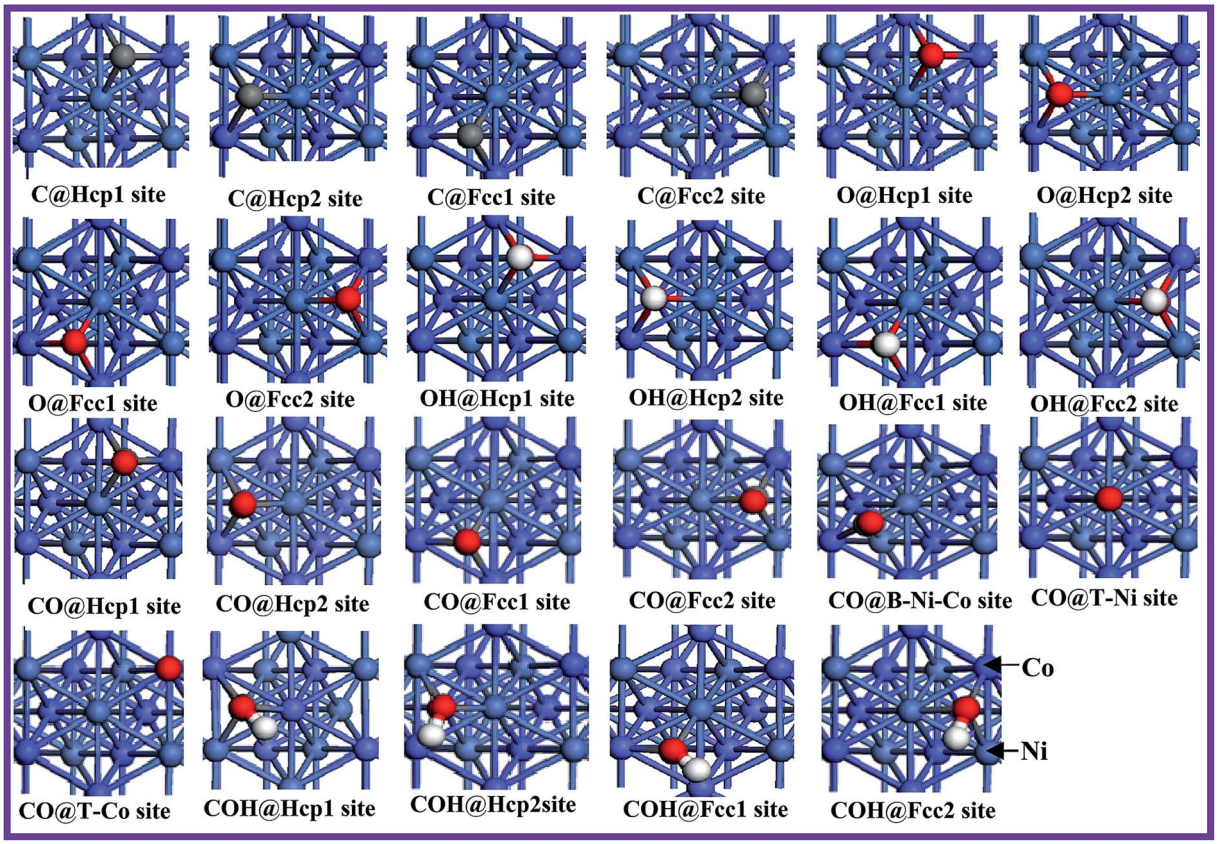

Fig. 3 The adsorption configurations of the species related to carbon elimination on Model A of CoNi(111). See Fig. 1 and 2 for color coding.

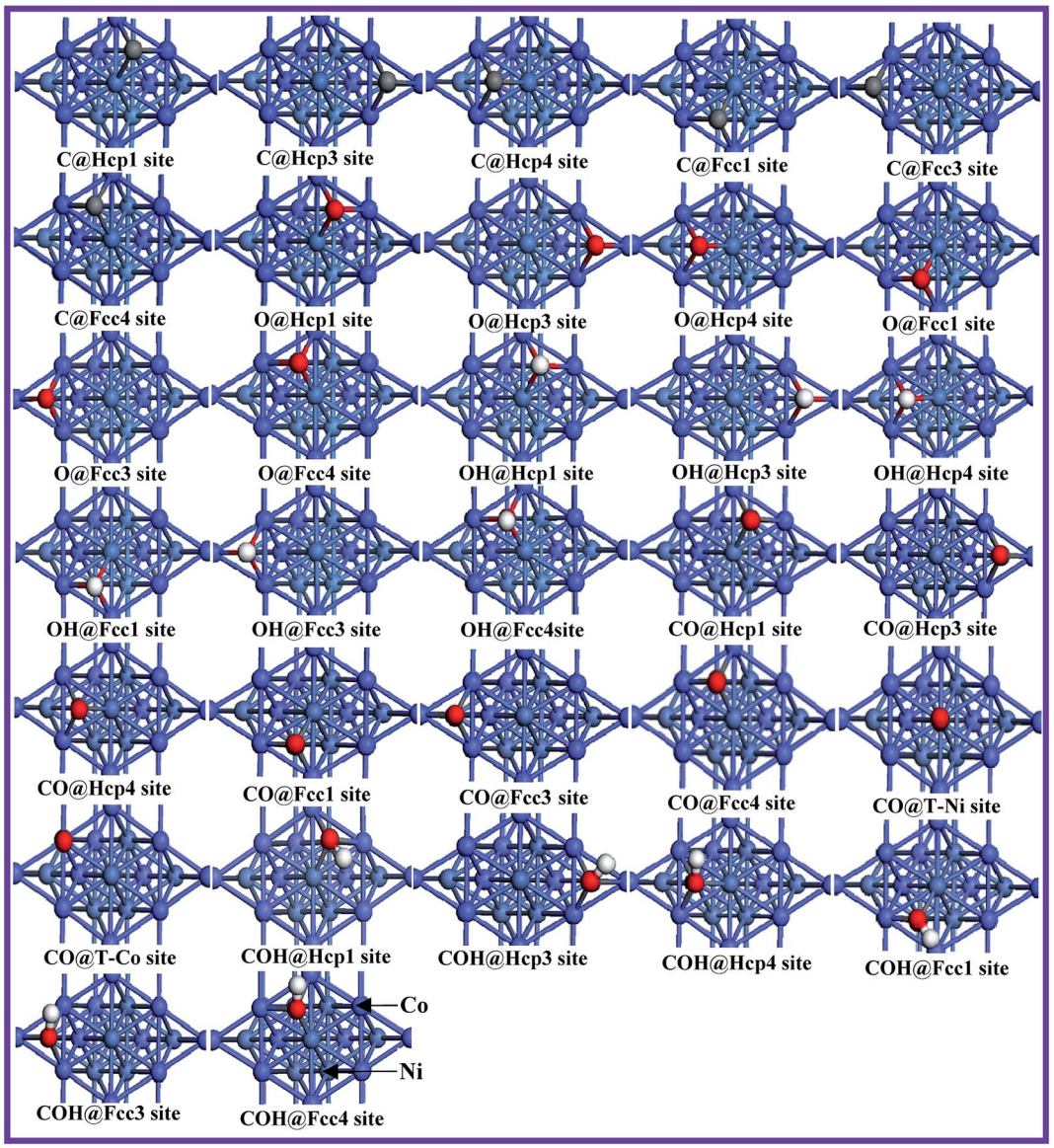

Fig. 4 The adsorption configurations of the species related to carbon elimination on Model B of CoNi(111). See Fig. 1 and 2 for color coding.

by 0.12 eV than that at the Hcp site. On CoNi(111), the most favorable O adsorption site for Models A–C is similar to the case of C atom adsorption on CoNi(111). We can see from Table 1 that the adsorption energy of the most stable adsorbed O increases from −5.76 eV on Ni(111), to −5.99 eV for Model A, to −6.12 eV for Model B, to −6.86 eV for Model C. Clearly, the introduction of Co significantly promotes the adsorption stability of O species.

On the other hand, O absorbed on Models B and C with the surface enrichment of Co is more favorable than that on Model A, and the increased degree of O adsorption energy far outstrips the corresponding values of C atom adsorption on Ni(111) and Models A–C, indicating that Co has a stronger affinity for oxygen species than carbon species. The stability order for all configurations on Model A is as follows: Hcp1 ≈ Fcc1 > Fcc2 ≈ Hcp2, that for Model B is Hcp3 ≈ Fcc3 > Fcc4 ≈ Fcc1 ≈ Hcp1 > Hcp4, and that for Model C is Hcp > Fcc1 ≈ Fcc2.

3.1.3 OH adsorption. OH is preferentially absorbed at the threefold site with the O–H bond oriented perpendicular to the Ni(111) and the three types of CoNi(111) surfaces. On Ni(111), OH binding at the Fcc site is more favored than that at the Hcp site. On Model A, four stable structures are verified; the most favorable adsorption site is the Fcc1 site with an adsorption energy of −3.68 eV. The other three adsorption energies are −3.64 eV at the Hcp1 site, −3.42 eV at the Hcp2, and −3.44 eV at the Fcc2, respectively. On Model B, there are six stable configurations at the threefold site; the Hcp3 and Fcc3 sites surrounded by three Co atoms are the most stable adsorption sites with equal adsorption energies of −3.79 eV, which is energetically more favorable than that for Model A. For Model C, OH binding at the Fcc1 site with the adsorption energy of −3.78 eV is slightly favored compared with those at the Hcp and Fcc2 sites. Our results indicate that the segregation of Co is beneficial for OH adsorption. Moreover, it is noteworthy that the

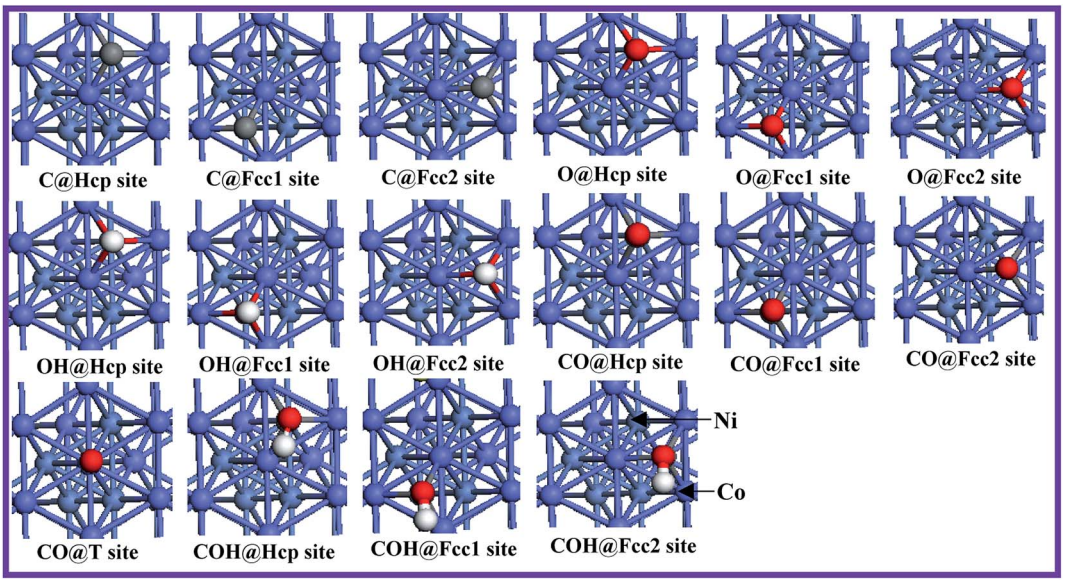

Fig. 5 The adsorption configurations of the species related to carbon elimination on Model C of CoNi(111). See Fig. 1 and 2 for color coding.

adsorption energies become more negative on the alloyed CoNi(111) surface compared to that on the pure Ni(111). Thus, the introduction of Co still enhances the adsorption ability of OH species.

3.1.4 COH adsorption. It is found that the initial adsorption configurations of COH at the top and bridge site are unstable, and COH species placed initially at these two sites are all relaxed to the threefold site after geometry optimization. From Table 1, we can see that the adsorption energies of COH binding at the threefold site on Ni(111), Model B and C are rather close (the energy difference is only within 0.06 eV), respectively, suggesting that there is no obvious site preference. However, on Model A, the most favorable COH adsorption site is the Hcp1 site, where the C atom is located at the center of the site, and the C–O bond is parallel to the surface normal. Further, the differences in adsorption energies are very small on Ni(111) and Models A–C (−4.39, −4.35, −4.43 and −4.49 eV, respectively), indicating that the introduction of Co has little effect on the adsorption stability of COH species.

3.1.5 CO adsorption. CO adsorption on the alloyed CoNi(111) and Ni(111) surfaces is different from the species mentioned above. CO located at the top site and bridge site can exist. On the Ni(111) surface, four stable adsorption configurations are obtained, and the corresponding adsorption energies are −1.89 eV at the Hcp site, −1.87 eV at the Fcc site, −1.76 eV at the bridge site, and −1.53 eV at the top site, respectively, which clearly show the order of adsorption energy: Hcp ≈ Fcc > bridge > top. On CoNi(111), there are seven stable configurations on Model A, eight stable configurations are verified on Model B, and four stable configurations are confirmed on Model C. CO binding at the Ni–Co bridge site on Model A exists, but CO located at other bridge sites on Models A–C tends to transfer to the stable threefold site after geometry optimization. On Models B, C and Ni(111), CO binding at the threefold site is preferred over those at the top and bridge sites, while for CO absorbed at the Ni–Co bridge site and Co top site on Model A, the adsorption energies differences are very small. Compared to Ni(111), it can be deduced that the introduction of Co into the Ni catalyst weakens the adsorption ability of CO, which agrees with the previous results obtained by experimental observation[31,35] and theoretical calculation.[34]

3.2 Mechanism for carbon elimination reactions of C + O and C + OH

3.2.1 Carbon elimination on Ni(111). Fig. 6 presents the configurations of the initial states (IS), transition states (TS), and final states (FS) for carbon elimination reactions of C + O and C + OH on Ni(111). C preferentially adsorbs at the Hcp and Fcc sites due to the small difference of adsorption energy, and O(OH) favorably binds at the Fcc site. Two stable co-adsorption structures of C and O(OH) are obtained, and chosen as the initial states; in the final states, since the difference in adsorption energy for CO(COH) species is very small between the Hcp and Fcc sites, CO(COH) species are located at the Hcp or Fcc site according to the corresponding IS configuration. The activation barriers and reaction energies for C + O and C + OH reactions are listed in Table 2.

(A) C + O reaction. As shown in Fig. 6, Path 1 is that the co-adsorbed C and O, which are absorbed at the Hcp and Fcc site, respectively, combine to form CO *via* TS1 along with O moving through the top of Ni, and the C–O distance is shortened from 3.21 Å in IS to 1.87 Å in TS1, and 1.19 Å in FS. This step is exothermic by 1.50 eV, and needs to overcome a high activation barrier of 2.29 eV. In Path 2, the co-adsorbed configuration of C and O atoms at two Fcc sites in a zigzag way is chosen as the initial state, and CO binding at the Hcp site is chosen as the final state; in TS2, the O atom transfers to the Ni–Ni bridge site, and the C atom is absorbed at its original site; the activation barrier of Path 2 *via* TS2 is 1.35 eV with the reaction energy of

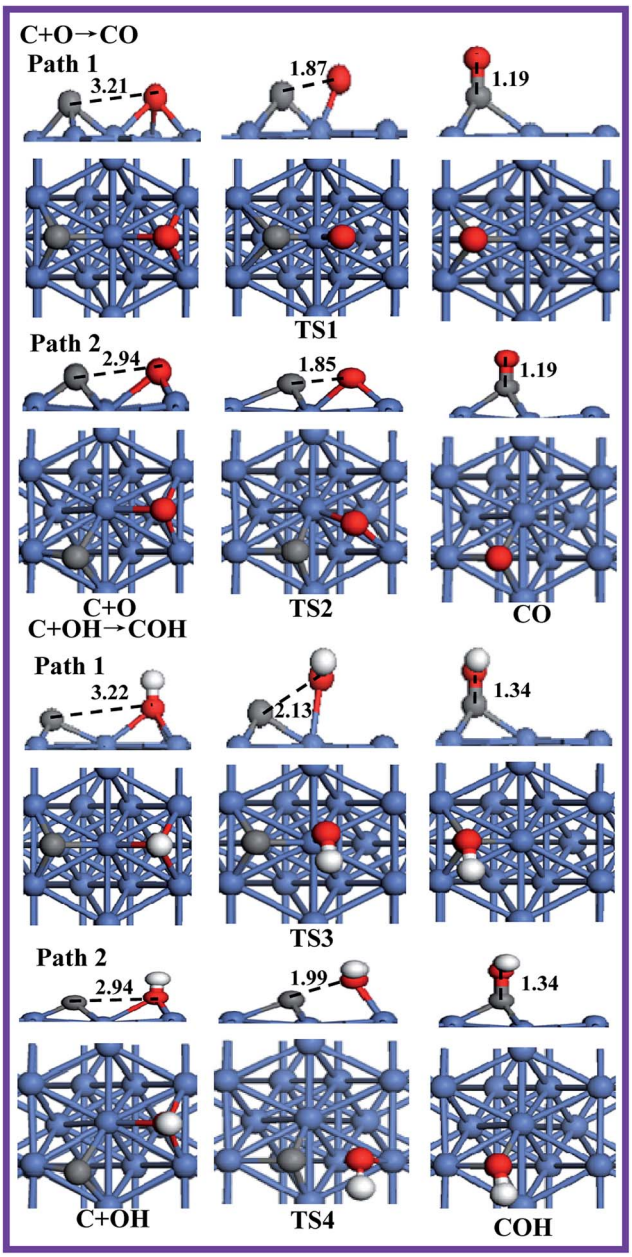

Fig. 6 Top views and side views for the structures of the initial states (IS), transition states (TS), and final states (FS) involved in carbon elimination on the Ni(111) surface. The unit of bond length is Å. See Fig. 1 and 2 for color coding.

−1.66 eV, which are lower than those of Path 1, namely, Path 2 is more favorable both thermodynamically and kinetically than Path 1.

(B) C + OH reaction. Similarly, two paths are considered for the C + OH reaction. In Path 1, C adsorbed at the Hcp site associates with OH at the Fcc site to form COH *via* TS3; in TS3, OH is located at the top of Co, C resides in its original site, and the C–O bond length is shortened from 3.22 Å in IS to 2.13 Å in TS3; this reaction is exothermic by 0.74 eV with an activation barrier of 1.26 eV. Path 2 involves C and OH co-adsorbing at two Fcc sites in a zigzag way, which can couple to form COH *via* TS4; in TS4, C is adsorbed at the Fcc site, and OH interacts with a Ni atom to approach the Hcp site. This reaction needs to overcome a low activation barrier of 1.06 eV with a reaction energy of −0.89 eV, which are lower than those of Path 1, namely, Path 2 is more favorable both thermodynamically and kinetically than Path 1.

The above results show that Path 2 is the most favorable pathway for both C + O and C + OH reactions. The activation barrier of the C + OH reaction is lower by 0.29 eV than that of the C + O reaction, which means that the OH species is more favorable for carbon elimination than O species.

On the other hand, our calculated activation barriers of the most favorable path for C + O and C + OH reactions on a $p((2 \times 2))$ Ni(111) surface are 1.35 eV and 1.06 eV, respectively, which are in agreement with the previous calculated values (1.33 eV and 1.20 eV)[21] with a $p(3 \times 3)$ Ni(111) surface. Meanwhile, discrepancies for the activation barriers of the C + O(OH) reaction exist due to the use of different sized Ni(111) surfaces; for example, Wang and co-workers[52] obtained an activation barrier of 0.64 eV for the C + O reaction on a three-layer $p(2 \times 2)$ model using DFT calculations. Liu *et al.*[34] used a similar model and methods, and obtained a larger activation barrier ($E_a = 0.86$ eV) for the C + O reaction. In other work, Zhu *et al.*[14] reported that the activation barrier of the C + O(OH) reaction is 1.59 eV (1.46 eV) using a periodic four-layer $p(3 \times 3)$ slab model, and both are reduced to 1.43 eV (1.34 eV) with the zero-point energy correction. The above studies suggested that the selected size of the model significantly affects the activation barriers of the C + O(OH) reaction. Moreover, there are large repulsive interactions between C and O(OH) in the co-adsorption configuration on a $p(2 \times 2)$ model, for example, the lateral interaction energies of C and O in the linear and zigzag modes are 0.58 and 1.01 eV, respectively. In contrast, for the same co-adsorption modes of C and O in our study, the lateral interaction energies are much lower (0.14 and 0.33 eV, respectively). Therefore, to avoid the uncertainty induced from the lateral interaction, we focus on our results calculated by using a $p(2\sqrt{3} \times 2)$ model.

3.2.2 Carbon elimination on Model A of CoNi(111). Our results show that on the homogeneous alloy CoNi surface, Model A, the most favorable adsorption site of C is the Hcp1 site, and O(OH) species preferentially absorb at the Hcp1 and Fcc1 sites due to the relatively small energy difference in adsorption energy. Two co-adsorption configurations of C and O(OH) are found, and selected as the initial states. The final states consist of CO adsorbed at the T-Co, B–Ni–Co and Hcp1 site (the energy difference is within 0.04 eV), and COH located at the Hcp1 site according to the corresponding IS configuration. The geometries and parameters of all possible transition states along the reaction of carbon elimination are presented in Fig. 7 and 8, respectively.

(A) C + O reaction. For the C + O reaction, six possible paths are mapped out. In Path 1, the co-adsorption of C and O sharing one Co atom in a zigzag way occurs at the Hcp1 site, and couples to produce CO adsorbed at the Hcp1 site *via* TS A1, in which C is located at its original site, and O transfers to the Ni–Co bridge site; the corresponding activation barrier and reaction energy are 1.52 and −1.13 eV, respectively. Path 2 is that C and O co-

Table 2 Calculated activation energies (E_a/eV) and reaction energies (ΔH/eV) of C + O and C + OH reactions on the pure Ni(111) and three types of alloyed CoNi(111) surfaces

		Ni(111)		CoNi(111)					
				Model A		Model B		Model C	
Reaction	Paths	E_a	ΔH	E_a	ΔH	E_a	ΔH	E_a	ΔH
C + O → CO	Path 1	2.29	−1.50	**1.52 (1.50)**[a]	**−1.13**	**1.50 (1.47)**	**−1.04**	**1.36 (1.33)**	**−1.02**
	Path 2	**1.35 (1.33)**	**−1.66**	1.61	−0.94	1.72	−0.77		
	Path 3			1.53	−1.12				
	Path 4			1.61	−0.93				
	Path 5			1.52	−1.10				
	Path 6			1.71	−0.92				
C + OH → COH	Path 1	1.26	−0.74	**1.19 (1.19)**	**−0.52**	**1.32 (1.30)**	**−0.44**	1.42	−0.24
	Path 2	**1.06 (1.04)**	**−0.89**	1.24	−0.50	1.43	−0.23	**1.40 (1.38)**	−0.34
	Path 3							1.41	−0.29

[a] The values presented in parentheses are the activation energies with ZPE correction.

adsorb at the Hcp1 and Fcc1 sites, respectively, and both react with each other to form CO *via* TS A2; in TS A2, the distance of C–O is shortened to 1.85 Å from 3.06 Å; this step is an exothermic process by 0.94 eV with an activation barrier of 1.61 eV. In Paths 3–6, the initial states of Paths 3 and 5 resemble that in Path 1, while those in Paths 4 and 6 are similar to that in Path 2. The final states of Paths 3 and 4 consist of CO adsorbed at the T-Co site, whereas Paths 5 and 6 take CO adsorbed at the Ni–Co bridge site as the final states. Four paths involve a similar transition state, whose geometry resembles those in Paths 1 and 2. The reaction barriers in Paths 3 and 5 are approximately equal, and are more favorable kinetically compared to Paths 4 and 6. Meanwhile, all reaction paths are exothermic, namely, they are thermodynamically favorable. In dynamics, Paths 1, 3 and 5 have the lowest reaction barriers among the six possible paths. Considering the reaction kinetics and thermodynamics, Path 1 is thought to be the most favorable path for C + O reaction to form CO on Model A.

(B) C + OH reaction. Two possible paths are conceived for C + OH reaction. The co-adsorbed structure of C + OH is similar to the co-adsorption of C + O in Paths 1 and 2. The final states consist of COH adsorbed at the Hcp1 site. In Paths 1–2, C associates with OH into COH *via* a similar transition state, in which OH transfers to the top of Co, and C is located at its original site. Our results show that Path 1 is more favorable kinetically than Path 2. Path 1 is exothermic by 0.52 eV with an activation barrier of 1.19 eV, which is lower than that of the most favorable path (1.52 eV) for C + O reaction. Obviously, the OH species is more preferred for carbon elimination than the O species on the homogeneous CoNi surface.

3.2.3 Carbon elimination on Model B of CoNi(111). On Model B, the C atom prefers to absorb at the Hcp3 and Hcp1 sites, O(OH) binding at the Hcp3 and Fcc3 sites is more favorable, and as a result, two stable co-adsorption structures of C and O(OH) are obtained, which are considered as the initial states of carbon elimination. The final states consist of CO and COH adsorbed at the Hcp1 and Hcp3 sites, respectively. The structures of the stationary states for the reaction of carbon elimination on Model B are displayed in Fig. 9.

(A) C + O reaction. Two possible paths are designed for C + O reaction. In Path 1, C and O co-adsorb at the Hcp1 site and Hcp3 site, respectively, and both can react to form CO adsorbed at the Hcp1 site *via* TS B1. In TS B1, O moves to the Co–Co bridge site, C leaves its original site, the distance of C–O is shortened to 1.80 Å in TS, and the forming C–O bond in FS is 1.20 Å; this reaction is exothermic by 1.04 eV with an activation barrier of 1.50 eV. In Path 2, the co-adsorption of C and O absorbed at the Hcp3 and Fcc3 sites can react to form CO absorbed at the Hcp3 site *via* TS B3; this reaction is exothermic by 0.77 eV with an activation barrier of 1.72 eV, which is higher by 0.22 eV than that in Path 1. As a result, considering the reaction kinetics and thermodynamics, Path 1 is more favorable both kinetically and thermodynamically than Path 2.

(B) C + OH reaction. Similarly, two possible paths are conceived for C + OH reaction. As displayed in Fig. 9, the co-adsorption structures of C + OH are similar to the corresponding structures of C + O, and COH is located at the Hcp1 and Hcp3 sites, respectively. Two paths involve a similar transition state, which resembles TS A5 on Model A. As listed in Table 2, Path 1 is more favorable both thermodynamically and kinetically than Path 2. Path 1 is exothermic by 0.44 eV with an activation barrier of 1.32 eV, which is lower by 0.18 eV than that of the most favorable path for C + O reaction. Therefore, the OH species has a stronger ability to eliminate carbon deposition than the O species on the CoNi alloy with the surface enrichment of Co.

3.2.4 Carbon elimination on Model C of CoNi(111). The geometries of the ISs, TSs, and FSs for C + O and C + OH reactions on Model C are presented in Fig. 10. The activation barriers and reaction energies are also listed in Table 2.

(A) C + O reaction. The co-adsorbed C and O binding at two Hcp sites in a zigzag mode is chosen as the IS, CO located at the Hcp site is chosen as the FS. The obtained TS configuration is similar to TS B2 on Model B, in which C is located at the Hcp site, and O is positioned at the adjacent Co–Co bridge site. This reaction is exothermic by 1.02 eV with an activation barrier of 1.36 eV.

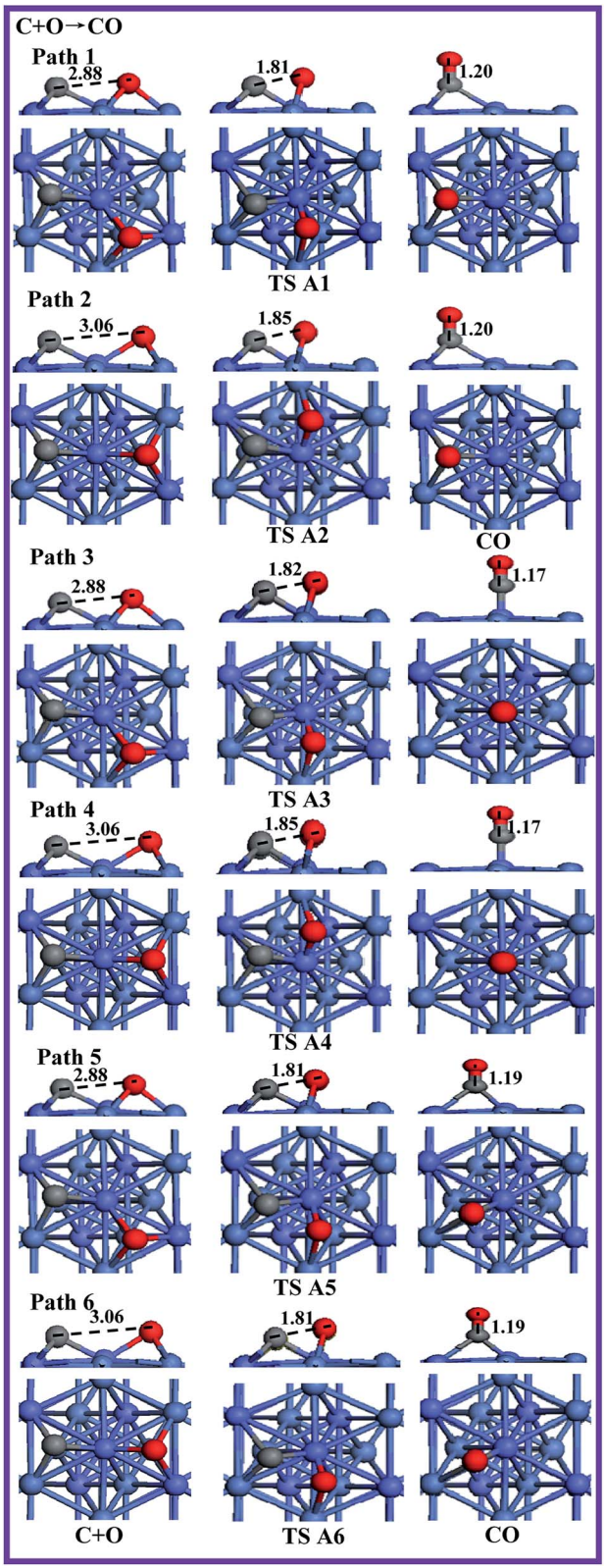

Fig. 7 Structures of the stationary states for C + O reaction on Model A of CoNi(111). See Fig. 1 and 2 for color coding.

(B) C + OH reaction. Three possible paths are conceived for C + OH reaction since OH positioned at the Fcc1, Hcp and Fcc2 sites have equal adsorption stabilities. Our results show that

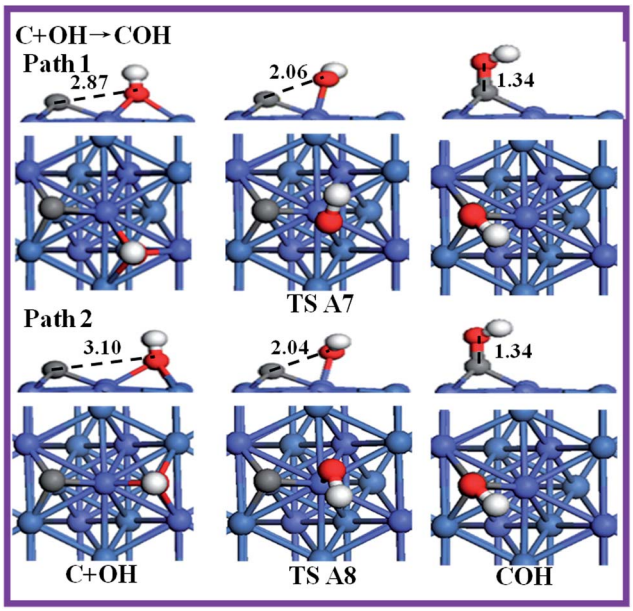

Fig. 8 Structures of the stationary states for the association of C + OH on Model A of CoNi(111). See Fig. 1 and 2 for color coding.

Path 2 is the most favorable reaction both thermodynamically and kinetically compared to Paths 1 and 3. Path 2 is exothermic by 0.34 eV with an activation barrier of 1.40 eV, which is larger than that of the C + O reaction, indicating that both O species have a relatively strong ability to remove carbon deposition on Model C with excessive segregation of Co.

3.3. Brief summary of the mechanism of C + O(OH) reaction

In order to elucidate the effect of different active component surfaces on carbon elimination, we compare the C + O and C + OH reactions on the alloyed CoNi(111) and the pure Ni(111) surfaces. The activation barrier and reaction energy for the most favorable path of the C + O and C + OH reactions on these different surfaces are also displayed in Table 2.

For the reaction C + O → CO, on Ni(111) surface, the most favorable path needs to overcome an activation barrier of 1.35 eV, which is lower than those on Models A and B by 0.17 and 0.15 eV, respectively, namely, when the Co surface coverage of the CoNi(111) surface is equal to 1/2 and 3/4 ML, the C + O reaction is obviously restrained. Meanwhile, the activation barrier of the C + O reaction on Model A is approximately equal to that on Model B, indicating that the moderate segregation of Co on the CoNi(111) alloy surface from 1/2 to 3/4 ML has little effect on the C + O reaction. However, the activation barrier of the most favorable path on Model C with the excessive segregation of Co is 1.36 eV, which is lower than those on Models A and B, suggesting that when Co surface coverage of the CoNi(111) surface is equal to 1 ML, the C + O reaction is accelerated on the alloy CoNi(111) surface. For the reaction C + OH → COH, the activation barrier (1.06 eV) of the most favorable path on Ni(111) is less than those on Models A–C (1.19, 1.32 and 1.40 eV, respectively), suggesting that as Co segregation increases, the C + OH reaction is obviously restrained. Further,

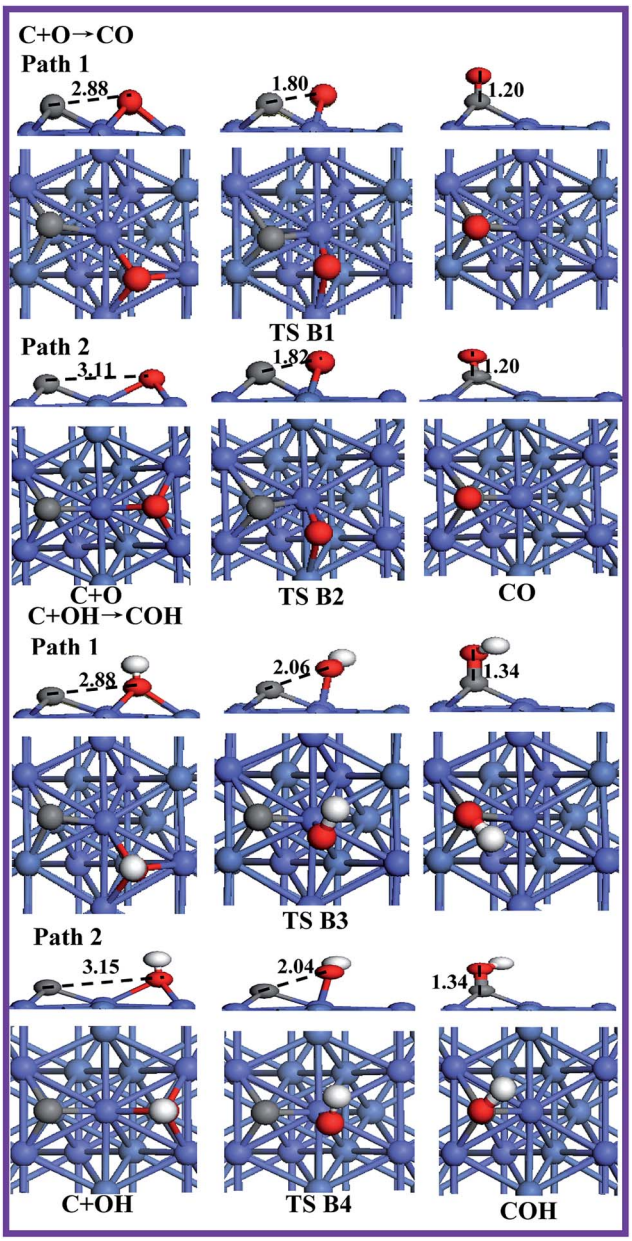

Fig. 9 Structures of the stationary states for C + O(OH) reaction on Model B of CoNi(111). See Fig. 1 and 2 for color coding.

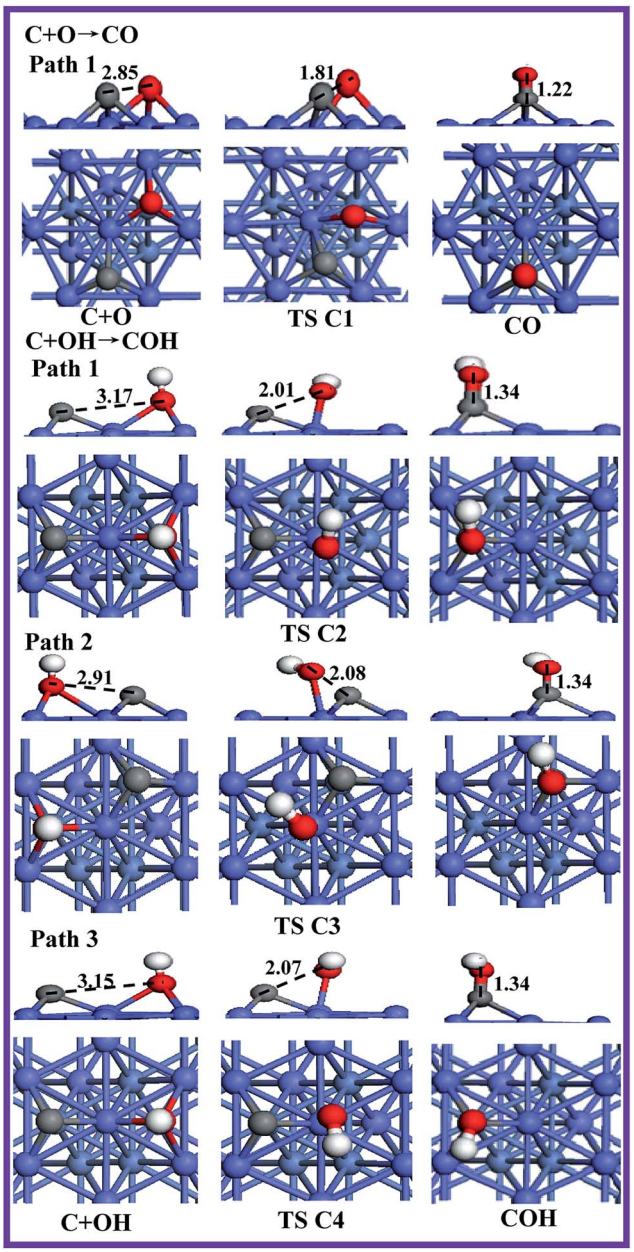

Fig. 10 Top views and side views of the structures of stationary states for carbon elimination on Model C of CoNi(111). See Fig. 1 and 2 for color coding.

our results show that compared to the Ni(111) surface, the reaction energy of C + O(OH) increases with the increasing Co surface coverage of the alloy CoNi(111) surface, namely, the exothermic energy decreases.

On the other hand, we can see from Table 2 that the activation barrier of the C + OH reaction is much lower than those of the C + O reaction on Ni(111), Models A and B, respectively, namely, when Co surface coverage is less than or equal to 3/4 ML, the OH species has a stronger ability to eliminate carbon than the O species. When the Co surface coverage of the CoNi(111) surface increases to 1 ML, the O species is slightly more favorable for carbon elimination than the OH species. Meanwhile, our results on the CoNi(111) surface show that the activation barrier of the C + O reaction on Model C with Co surface coverage of 1 ML is much larger than that of the C + OH reaction on Model A with Co surface coverage of 1/2 ML. Therefore, for carbon elimination on the CoNi alloy surface, OH species should serve as the key species for carbon elimination rather than O species, and the Co surface coverage of CoNi(111) surface should be kept 1/2 ML.

3.4. Effect of temperature on C + O and C + OH reactions

Previous studies have reported that catalytic reforming of CH_4 with CO_2 is a highly endothermic reaction, which requires operating temperatures of 800–1000 K to obtain the high

Table 3 The rate constant k (s^{-1}) for C + O(OH) reaction at different temperatures on the pure Ni(111) and the alloyed CoNi(111) surfaces

		Rate constant k (s^{-1})				
Surface	Reaction	800 K	850 K	900 K	950 K	1000 K
Ni(111)	C + O → CO	9.38×10^4	3.15×10^5	9.28×10^5	2.45×10^6	5.87×10^6
	C + OH → COH	6.59×10^6	1.72×10^7	4.06×10^7	8.77×10^7	1.76×10^8
Model A	C + O → CO	8.7×10^3	3.38×10^4	1.13×10^5	3.34×10^5	8.89×10^5
	C + OH → COH	4.85×10^5	1.42×10^6	3.72×10^6	8.83×10^6	1.93×10^7
Model B	C + O → CO	2.89×10^4	1.1×10^5	3.61×10^5	1.05×10^6	2.75×10^6
	C + OH → COH	5.11×10^5	1.67×10^6	4.78×10^6	1.23×10^7	2.89×10^7
Model C	C + O → CO	1.88×10^5	6.36×10^5	1.88×10^6	4.97×10^6	1.2×10^7
	C + OH → COH	1.96×10^5	6.9×10^5	2.11×10^6	5.75×10^6	1.42×10^7

equilibrium conversion of CH_4 and CO_2 to H_2 and CO, and to minimize the thermodynamic driving force for carbon deposition.[53] Therefore, to further understand the effect of temperature on the reactions of C + O(OH) on Ni(111) and the alloyed CoNi(111) surfaces, we have calculated the rate constants of the most favorable path of C + O(OH) reaction at the temperatures of 800, 850, 900, 950 and 1000 K, respectively, and the corresponding results are listed in Table 3. A detailed description of the rate constant calculation has been given in the ESI.†

From Table 3, we can see that the rate constant k of the C + O(OH) reaction increases rapidly as the temperature increases on Ni(111) and the alloyed CoNi(111) surfaces; at the same temperature, the rate constant of the C + OH reaction is larger than that of the C + O reaction on the same catalyst surface, indicating that the OH species has a stronger ability to eliminate carbon than the O species. For C + O reaction, at the same temperature, the rate constants are in the order Model C > Ni(111) > Model B > Model A, which shows that the C + O reaction is obviously restrained on Models A–B, however, compared to the Ni(111) surface, the C + O reaction is accelerated on Model C. Namely, when the Co surface coverage reaches 1 ML, the carbon elimination ability of the C + O reaction on the alloy CoNi surface is more favorable than that on the Ni(111) surface. For the C + OH reaction, the rate constants are in the order Ni(111) > Model B > Model A > Model C at the same temperature, which means that compared to Ni(111), the C + OH reaction is obviously restrained on Models A–C; further, the rate constants of the C + OH reaction on Model B are much larger than that of the C + O reaction on Model C.

As a result, for carbon elimination on the CoNi alloy surface, OH species should serve as the key species for carbon elimination, and the Co surface coverage of the CoNi(111) surface should be kept at 3/4 ML, which is different from the results obtained from the activation barrier. The discrepancies may be because the activation barrier is calculated at a temperature of 0 K, but the rate constants are calculated at a temperature of 800–1000 K, indicating that reaction temperature obviously affects the kinetics of C + O(OH) reaction under realistic conditions.

4. Conclusions

In this work, we have carried out a systematic DFT study to investigate the adsorption of C, OH, O, COH and CO species involved in carbon elimination, as well as the mechanism of C + O(OH) reaction on three types of alloyed CoNi(111) surface and the pure Ni(111) surface. For the alloyed CoNi(111) surface, three models, the homogeneous surface (Model A), the surface with moderate segregation of Co (Model B), and the surface with excessive segregation of Co (Model C), have been constructed to represent a CoNi(111) surface with different surface Co segregation. Our results show that compared to the pure Ni(111), the incorporation of Co into the Ni catalyst increases the adsorption stability of the C, O and OH species, but weakens the adsorption stability of CO species, and has little effect on COH adsorption. Meanwhile, Co has a stronger affinity for oxygen species than carbon species. On the other hand, the mechanism and rate constants of C + O(OH) reaction show that the OH species is more favorable for carbon elimination than O species on Ni(111) and the alloy CoNi(111) surfaces; on the alloy CoNi(111) surface, when Co surface coverage is equal to 1 ML, compared to Ni(111), the C + O reaction can be accelerated. For the C + OH reaction, on CoNi(111) surface, when the Co surface coverage is equal to 3/4 ML, the C + OH reaction is obviously favorable according to the rate constant calculations. Further, the rate constants of the C + OH reaction on the CoNi(111) with Co surface coverage of 3/4 ML is much larger than that of the C + O reaction on CoNi(111) with Co surface coverage of 1 ML, suggesting that OH species should serve as the key species for carbon elimination on the alloy CoNi surface, and the Co surface coverage of CoNi(111) surface should be kept at 3/4 ML for carbon elimination on the alloy CoNi surface.

Acknowledgements

This work is financially supported by the National Natural Science Foundation of China (no. 21276171, 21276003 and 21476155), the Natural Science Foundation of Shanxi Province (no. 2014011012-2) and the Top Young Innovative Talents of Shanxi.

References

1 M. S. Fan, A. Z. Abdullah and S. Bhatia, Catalytic Technology for Carbon Dioxide Reforming of Methane to Synthesis Gas, *ChemCatChem*, 2009, **1**, 192–208.

2 M. C. J. Bradford and M. A. Vannice, CO_2 Reforming of CH_4, *Catal. Rev.*, 1999, **41**, 1–42.
3 J. M. Ginsburg, J. Piña, T. E. Solhet and H. I. Lasa, Coke Formation over a Nickel Catalyst under Methane Dry Reforming Conditions: Thermodynamic and Kinetic Models, *Ind. Eng. Chem. Res.*, 2005, **44**, 4846–4854.
4 K. Tomishige, Y. G. Chen, K. Yokoyama and K. Fujimoto, Catalytic Performance and Catalyst Structure of Nickel–Magnesia Catalysts for CO_2 Reforming of Methane, *J. Catal.*, 1999, **184**, 479–490.
5 D. Cheng, X. Zhu and Y. Ben, Carbon Dioxide Reforming of Methane over Ni/Al_2O_3 Treated with Glow Discharge Plasma, *Catal. Today*, 2006, **115**, 205–210.
6 S. Tang, L. Ji, J. Lin, H. C. Zeng, K. L. Tan and K. Li, CO_2 Reforming of Methane to Synthesis Gas over Sol–Gel-made Ni/γ-Al_2O_3 Catalysts from Organometallic Precursors, *J. Catal.*, 2000, **194**, 424–430.
7 J. H. Kim, D. J. Suh, T. J. Park and K. L. Kim, Effect of Metal Particle Size on Coking during CO_2 Reforming of CH_4 over Ni–Alumina Aerogel Catalysts, *Appl. Catal., A*, 2000, **197**, 191–200.
8 J. Zhang, H. Wang and A. K. Dalai, Effects of Metal Content on Activity and Stability of Ni-Co Bimetallic Catalysts for CO_2 Reforming of CH_4, *Appl. Catal., A*, 2008, **339**, 121–129.
9 S. Vasileiadis and Z. Ziaka-Vasileiadou, Biomass Reforming Process for Integrated Solid Oxide-Fuel Cell Power Generation, *Chem. Eng. Sci.*, 2004, **59**, 4853–4859.
10 D. L. Trimm, Coke Formation and Minimisation during Steam Reforming Reactions, *Catal. Today*, 1997, **37**, 233–238.
11 M. Rezaei, S. M. Alavi, S. Sahebdelfar and Z. F. Yan, Nanocrystalline Zirconia as Support for Nickel Catalyst in Methane Reforming with CO_2, *Energy Fuels*, 2006, **20**, 923–929.
12 Y. Li, Y. Wang, X. Zhang and Z. Mi, Thermodynamic Analysis of Autothermal Steam and CO_2 Reforming of Methane, *Int. J. Hydrogen Energy*, 2008, **33**, 2507–2514.
13 M. Maestri, D. G. Vlachos, A. Beretta and G. Gropp, Steam and Dry Reforming of Methane on Rh: Microkinetic Analysis and Hierarchy of Kinetic Models, *J. Catal.*, 2008, **259**, 211–222.
14 Y. A. Zhu, D. Chen, X. G. Zhou and W. K. Yuan, DFT Studies of Dry Reforming of Methane on Ni Catalyst, *Catal. Today*, 2009, **148**, 260–267.
15 F. Solymosi, P. Tolmacsov and T. S. Zaka, Dry Reforming of Propane over Supported Re Catalyst, *J. Catal.*, 2005, **233**, 51–59.
16 A. Siahvashi and A. A. Adesina, Kinetic Study of Propane CO_2 Reforming over Bimetallic Mo–Ni/Al_2O_3 Catalyst, *Ind. Eng. Chem. Res.*, 2013, **52**, 15377–15386.
17 D. Sutton, J. F. Moisan and J. R. H. Ross, Kinetic Study of CO_2 Reforming of Propane over Ru/Al_2O_3, *Catal. Lett.*, 2001, **75**, 175–181.
18 P. Ferreira-Aparicio, I. Rodrıguez-Ramos, J. A. Anderson and A. Guerrero-Ruiz, Mechanistic Aspects of the Dry Reforming of Methane over Ruthenium Catalysts, *Appl. Catal., A*, 2000, **202**, 183–196.
19 M. A. Goula, A. A. Lemonidou and A. M. Efstathiouy, Characterization of Carbonaceous Species Formed during Reforming of CH_4 with CO_2 over Ni/CaO-Al_2O_3 Catalysts Studied by Various Transient Techniques, *J. Catal.*, 1996, **161**, 626–640.
20 M. Shishkin and T. Ziegler, Coke-Tolerant $Ni/BaCe1–xY_xO_3–\delta$ Anodes for Solid Oxide Fuel Cells: DFT+U Study, *J. Phys. Chem. C*, 2013, **117**, 7086–7096.
21 S. G. Wang, D. B. Cao, Y. W. Li, J. Wang and H. Jiao, Reactivity of Surface OH in CH_4 Reforming Reactions on Ni(111): A Density Functional Theory Calculation, *Surf. Sci.*, 2009, **603**, 2600–2606.
22 Z. Hou and T. Yashima, Small Amounts of Rh-Promoted Ni Catalysts for Methane Reforming with CO_2, *Catal. Lett.*, 2003, **89**, 193–197.
23 X. Li, J. Ai, W. Li and D. Li, Ni-Co Bimetallic Catalyst for CH_4 Reforming with CO_2, *Front. Chem. Eng. China*, 2010, **4**, 476–480.
24 K. Nagaoka, K. Takanabe and K. Aika, Modification of Co/TiO_2 for Dry Reforming of Methane at 2MPa by Pt, Ru or Ni, *Appl. Catal., A*, 2004, **268**, 151–158.
25 D. San-José-Alonso, J. Juan-Juan, M. J. Illán-Gómez and M. C. Román-Martínez, Ni, Co and Bimetallic Ni–Co Catalysts for the Dry Reforming of Methane, *Appl. Catal., A*, 2009, **371**, 54–59.
26 W. C. Conner Jr, G. M. Pajonk and S. J. Teichner, Spillover of Sorbed Species, *Adv. Catal.*, 1986, **34**, 1–79.
27 W. C. Conner Jr and J. L. Falconer, Spillover in Heterogeneous Catalysis, *Chem. Rev.*, 1995, **95**, 759–788.
28 A. C. W. Koh, L. Chen, K. W. Leong and B. F. G. Johnson, Hydrogen or Synthesis Gas Production *via* the Partial Oxidation of Methane over Supported Nickel–Cobalt Catalysts, *Int. J. Hydrogen Energy*, 2007, **32**, 725–730.
29 J. Zhang, H. Wang and A. K. Dalai, Development of Stable Bimetallic Catalysts for Carbon Dioxide Reforming of Methane, *J. Catal.*, 2007, **249**, 300–310.
30 L. Chen, Q. Zhu and R. Wu, Effect of Co–Ni Ratio on the Activity and Stability of Co–Ni Bimetallic Aerogel Catalyst for Methane Oxy-CO_2 Reforming, *Int. J. Hydrogen Energy*, 2011, **36**, 2128–2136.
31 K. Takanabe, K. Nagaoka and K. Nariai, Titania-Supported Cobalt and Nickel Bimetallic Catalysts for Carbon Dioxide Reforming of Methane, *J. Catal.*, 2005, **232**, 268–275.
32 P. Djinović, I. G. O. Črnivec, B. Erjavec and A. Pintar, Details Behind the Self-Regeneration of Supported $NiCo/Ce_{0.8}Zr_{0.2}O_2$ Bimetallic Catalyst in the CH_4–CO_2 Reforming Reaction, *ChemCatChem*, 2014, **6**, 1652–1663.
33 J. Xu, W. Zhou, Z. Li, J. Wang and J. Ma, Biogas Reforming for Hydrogen Production over Nickel and Cobalt Bimetallic Catalysts, *Int. J. Hydrogen Energy*, 2009, **34**, 6646–6654.
34 H. Liu, R. Zhang, F. Ding, R. Yan, B. Wang and K. Xie, A First-Principles Study of C + O Reaction on NiCo(111) Surface, *Appl. Surf. Sci.*, 2011, **257**, 9455–9460.
35 K. Takanabe, K. Nagaoka and K. Nariai, Improved Resistance Against Coke Deposition of Titania Supported Cobalt and Nickel Bimetallic Catalysts for Carbon Dioxide Reforming of Methane, *Catal. Lett.*, 2005, **102**, 153–157.

36 H. Zhang, T. Yao, Z. Sun, Y. Li, Q. Liu and F. Hu, Structural Study on Co–Ni Bimetallic Nanoparticles by X-ray Spectroscopy, *J. Phys. Chem. C*, 2010, **114**, 13596–13600.
37 G. Kresse and J. Furthmüller, Efficient Iterative Schemes for *Ab Initio* Total-Energy Calculations Using a Plane-Wave Basis Set, *Phys. Rev. B: Condens. Matter Mater. Phys.*, 1996, **54**, 11169–11186.
38 G. Kresse and J. Furthmüller, Efficiency of *Ab Initio* Total Energy Calculations for Metals and Semiconductors Using a Plane-Wave Basis Set, *Comp. Mater. Sci.*, 1996, **6**, 15–50.
39 G. Kresse and J. Hafner, Ab Initio Molecular Dynamics for Open-Shell Transition Metals, *Phys. Rev. B: Condens. Matter Mater. Phys.*, 1993, **48**, 13115–13118.
40 J. A. White and D. M. Bird, Implementation of Gradient-Corrected Exchange-Correlation Potentials in Car-Parrinello Total-Energy Calculations, *Phys. Rev. B: Condens. Matter Mater. Phys.*, 1994, **50**, 4954–4957.
41 P. E. Blochl, Projector Augmented-Wave Method, *Phys. Rev. B: Condens. Matter Mater. Phys.*, 1994, **50**, 17953–17979.
42 J. P. Perdew, K. Burke and M. Ernzerhof, Generalized Gradient Approximation Made Simple, *Phys. Rev. Lett.*, 1996, **77**, 3865–3868.
43 D. J. Chadi, Special Points for Brillouin-Zone Integrations, *Phys. Rev. B: Condens. Matter Mater. Phys.*, 1977, **16**, 1746–1747.
44 M. Methfessel and A. T. Paxton, High-Precision Sampling for Brillouin-Zone Integration in Metals, *Phys. Rev. B: Condens. Matter Mater. Phys.*, 1989, **40**, 3616–3621.
45 W. An, X. C. Zeng and C. H. Turner, First-Principles Study of Methane Dehydrogenation on a Bimetallic Cu/Ni (111) surface, *J. Chem. Phys.*, 2009, **131**, 174702.
46 C. Kittel and P. McEuen, *Introduction to Solid State Physics*, Wiley, New York, 1976.
47 D. Sheppard, P. Xiao, P. Chemelewski, D. D. Johnson and G. Henkelman, Generalized Solid-State Nudged Elastic Band Method, *J. Chem. Phys.*, 2012, **136**, 074103.
48 D. Sheppard, R. Terrell and G. Henkelman, Optimization Methods for Finding Minimum Energy Paths, *J. Chem. Phys.*, 2008, **128**, 134106.
49 G. Henkelman and H. Jónsson, A Dimer Method for Finding Saddle Points on High Dimensional Potential Surfaces Using Only First Derivatives, *J. Chem. Phys.*, 1999, **111**, 7010–7022.
50 R. A. Olsen, G. J. Kroes and G. Henkelman, Jónsson H. Comparison of Methods for Finding Saddle Points without Knowledge of the Final States, *J. Chem. Phys.*, 2004, **121**, 9776–9792.
51 S. G. Wang, D. B. Cao, Y. W. Li, J. Wang and H. Jiao, CO_2 Reforming of CH_4 on Ni (111): A Density Functional Theory Calculation, *J. Phys. Chem. B*, 2006, **110**, 9976–9983.
52 S. G. Wang, X. Y. Liao, J. Hu, D. B. Cao, Y. W. Li and J. Wang, Kinetic Aspect of CO_2 Reforming of CH_4 on Ni(111):A Density Functional Theory Calculation, *Surf. Sci.*, 2007, **601**, 1271–1284.
53 C. Liu, J. Ye, J. Jiang and Y. Pan, Progresses in the preparation of coke resistant Ni-based catalyst for steam andCO_2 reforming of methane, *ChemCatChem*, 2011, **3**, 529–541.

